Exact and approximate postform distorted-wave Born approximation amplitudes for the Coulomb breakup of neutron halo nuclei

M. Zadro*
Rudjer Bošković Institute, P.O. Box 180, 10002 Zagreb, Croatia
(Received 18 April 2002; published 4 September 2002)

The Coulomb breakup of neutron halo nuclei is considered within the framework of the postform distorted-wave Born approximation (DWBA). The quality of commonly used additional approximations to the DWBA theory is investigated by comparing the approximate with the exact DWBA calculations. The exact DWBA amplitude is expressed in momentum space as a three-dimensional integral and evaluated numerically. Calculations are presented for the Coulomb breakup of deuteron and ^{11}Be at very forward angles at the beam energy of ~ 70 MeV/nucleon. The factorization approximation to the DWBA amplitude is studied and found to be suspected.

DOI: 10.1103/PhysRevC.66.034603 PACS number(s): 24.10.Eq, 25.60.Gc, 25.70.De

I. INTRODUCTION

Neutron halo nuclei are very weakly bound two-body systems consisting of a charged core, with normal nuclear density, and a valence neutron (or pair of neutrons), e.g., Refs. [1–3]. The loosely bound valence neutron(s) extend far out in space surrounding the core and form a diffuse halo. A unique signature of such nuclei is the large total reaction cross section [4,5]. The Coulomb breakup is a significant reaction channel for highly charged targets [6–9]. The study of the Coulomb breakup reactions provides informations on the structure of these nuclei.

There has been a number of different theoretical analyses, both semiclassical and quantum mechanical, of the Coulomb breakup of neutron halo nuclei. In the first-order semiclassical perturbation theory of Coulomb excitation [10,11] the breakup cross section is directly related to the electromagnetic transition matrix element, which contains information on the projectile ground state wave function. For example, the one-neutron halo nuclei ^{11}Be and ^{19}C have been studied in this way [8,9]. Various approaches have been used to take into account higher order effects. The main methods in the semiclassical description of the breakup process are the coupled-channel calculations [12,13], the direct numerical integration of the time dependent Schrödinger equation for the relative motion of the core and halo [14–20], and explicit inclusion of higher order terms [21,22]. In these semiclassical approaches classical trajectories are used to describe the relative motion between the projectile and the target.

Another approach for the analysis of the Coulomb breakup reactions is a fully quantum mechanical treatment in the postform distorted-wave Born approximation (DWBA) theory [23]. The theory is first order in the interaction between the core and valence particle but the interaction between the core and target is taken into account to all orders. However, in applications of this theory to the Coulomb breakup of neutron halo nuclei the finite-range transition amplitude has not been calculated exactly. The additional approximations have been used, such as the Baur-Trautmann approximation [24] or the local momentum approximations [25–27], where the finite-range effects are included approximately.

Recently, an adiabatic theory of the Coulomb breakup of neutron halo nuclei has been developed [25,28]. It includes the initial and final state interactions to all orders. The theory leads to an expression for the breakup amplitude similar to forms obtained using approximations to the DWBA theory. However, assumptions underlying the two theories are quite different [25]. While the adiabatic approach assumes that excitation of the projectile is to the low-energy continuum, the DWBA assumes that excitation of the projectile is weak and so needs be treated only to first order.

Several calculations of the Coulomb breakup of ^{11}Be and ^{19}C, based on the DWBA with an effective momentum approximation, have been reported recently [25–27]. The results have been compared with those obtained within the adiabatic breakup theory. In most of the cases studied the two theoretical approaches produced similar results. However, since the DWBA breakup amplitude has not been evaluated exactly, conclusions suggested by such a comparison, regarding the assumptions made in the two theories, are questionable.

In this paper, we reexamine approximate methods for the calculations of the Coulomb breakup of neutron halo nuclei in the framework of the postform DWBA theory. The theory is applied to the deuteron, as an example of a loosely bound two-body system, and to the one-neutron halo nucleus ^{11}Be. The results of the exact DWBA calculations for the breakup into very forward angles, at the beam energy of ~ 70 MeV/nucleon, are presented and compared with those obtained using different simplifying approximations. Comparisons of the exact DWBA calculations with experimental data, or with the results of other theories of the Coulomb breakup, are outside the scope of this work.

In Sec. II the theoretical formalism is given. Calculations are presented and discussed in Sec. III. Summary and conclusions are given in Sec. IV.

II. FORMALISM

We consider the reaction $p+t \rightarrow c+n+t$, where the two-body composite projectile $p=c+n$, of charge Z_p, breaks up

*Email address: zadro@rudjer.irb.hr

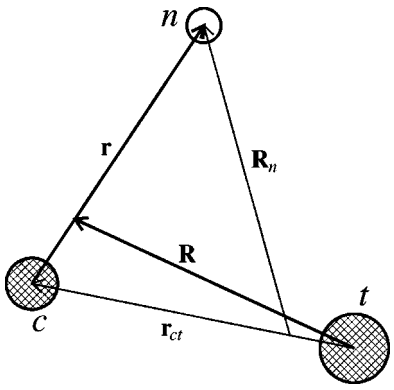

FIG. 1. Definition of the coordinate vectors used in the text. *c*, *n*, and *t* represent the charged core, the neutral valence particle, and the target, respectively.

into the charged fragment *c* and the neutral particle *n* in the Coulomb field of a target *t*, of charge Z_t; (see, e.g., Refs. [25,26]). The total angular momentum of the particle *p* is J_p, with projection M_p. The spins of the fragments *c* and *n* are J_c and *S*, with projections M_c and σ, respectively. The target is assumed spinless. The internal wave functions of the particles are denoted by $\Phi(\xi)$, where ξ are the internal coordinates. The particle masses are $m_p = m_c + m_n$ and m_t.

The coordinates used to describe the reaction are shown in Fig. 1. The incident momentum of the projectile in the center of mass (c.m.) frame of the projectile and target is $\hbar\mathbf{K}_i$. The momenta corresponding to $\mathbf{r}$, $\mathbf{R}$, $\mathbf{r}_{ct}$, and $\mathbf{R}_n$ in the final channel are $\hbar\mathbf{k}$, $\hbar\mathbf{K}_f$, $\hbar\mathbf{k}_{ct}$, and $\hbar\mathbf{K}_n$, respectively. The position vectors and the wave vectors satisfy the following relations:

$$\mathbf{r}_{ct} = \mathbf{R} - \alpha\mathbf{r}, \quad \mathbf{R}_n = \beta\mathbf{R} + \gamma\mathbf{r}, \tag{1}$$

$$\mathbf{k}_{ct} = \gamma\mathbf{K}_f - \beta\mathbf{k}, \quad \mathbf{K}_n = \alpha\mathbf{K}_f + \mathbf{k}, \tag{2}$$

where

$$\alpha = \frac{m_n}{m_c + m_n}, \quad \beta = \frac{m_t}{m_c + m_t}, \quad \gamma = 1 - \alpha\beta. \tag{3}$$

The interactions involved are the core-valence particle binding potential $V_{nc}(\mathbf{r})$ and the core-target point Coulomb potential $V_{ct}(\mathbf{r}_{ct})$.

The exact *T*-matrix element in the postform is given by

$$T_{M_c\sigma;M_p} = \langle \chi^{(-)}(\mathbf{k}_{ct},\mathbf{r}_{ct})\Phi_{J_cM_c}(\xi_c)e^{i\mathbf{K}_n\cdot\mathbf{R}_n}\Phi_{S\sigma}(\xi_n)| \times V_{nc}(\mathbf{r})|\Psi^{(+)}_{J_pM_p}(\xi_c,\xi_n,\mathbf{r},\mathbf{R})\rangle. \tag{4}$$

Here $\Psi^{(+)}_{J_pM_p}(\xi_c,\xi_n,\mathbf{r},\mathbf{R})$ is the full solution of the three-body scattering problem with the system $p+t$ in the initial channel and with outgoing spherical waves. The $\chi^{(-)}(\mathbf{k}_{ct},\mathbf{r}_{ct})$ is the Coulomb distorted wave function with incoming spherical waves, describing the *c*-*t* relative motion in the final state. Since $V_{nt}=0$, the particle *n* is described by the plane wave in the final state.

In the DWBA the full solution $\Psi^{(+)}$ is approximated by the product

$$\Psi^{(+)}_{J_pM_p}(\xi_c,\xi_n,\mathbf{r},\mathbf{R}) \approx \Phi_{J_pM_p}(\xi_c,\xi_n,\mathbf{r})\chi^{(+)}(\mathbf{K}_i,\mathbf{R}), \tag{5}$$

where $\Phi_{J_pM_p}(\xi_c,\xi_n,\mathbf{r})$ is the ground state wave function of the projectile and $\chi^{(+)}(\mathbf{K}_i,\mathbf{R})$ is the Coulomb distorted wave describing the relative motion of the c.m. of the projectile with respect to the target, with outgoing spherical waves. The integral over the internal coordinates in Eq. (4) can be expressed as

$$\langle \Phi_{J_cM_c}(\xi_c)\Phi_{S\sigma}(\xi_n)|\Phi_{J_pM_p}(\xi_c,\xi_n,\mathbf{r})\rangle = \sum_{lmj\mu} S^{1/2}_{lj}\langle J_cM_cj\mu|J_pM_p\rangle\langle lmS\sigma|j\mu\rangle\Phi^{lm}_p(\mathbf{r}). \tag{6}$$

Here $S^{1/2}_{lj}$ is the usual spectroscopic amplitude and $\Phi^{lm}_p(\mathbf{r})$ is the wave function of the relative motion of the fragments *c* and *n* in the ground state of the projectile *p*,

$$\Phi^{lm}_p(\mathbf{r}) = i^l u_l(r) Y_{lm}(\hat{\mathbf{r}}), \tag{7}$$

where $u_l(r)$ is the radial wave function and $Y_{lm}(\hat{\mathbf{r}})$ is the spherical harmonic. In Eqs. (6) and (7), *l* is the orbital angular momentum of the relative motion between particles *c* and *n*, and *j* is the total angular momentum of the particle *n* in the ground state of the particle $p = c + n$.

Using Eq. (6) the *T* matrix can be written as

$$T_{M_c\sigma;M_p} = \sum_{lmj\mu} S^{1/2}_{lj}\langle J_cM_cj\mu|J_pM_p\rangle\langle lmS\sigma|j\mu\rangle B_{lm}, \tag{8}$$

where the reduced transition amplitude B_{lm} is

$$B_{lm} = \langle \chi^{(-)}(\mathbf{k}_{ct},\mathbf{r}_{ct})e^{i\mathbf{K}_n\cdot\mathbf{R}_n}|V_{nc}(\mathbf{r})|\Phi^{lm}_p(\mathbf{r})\chi^{(+)}(\mathbf{K}_i,\mathbf{R})\rangle. \tag{9}$$

The triple differential cross section of the reaction is given by

$$\frac{d^3\sigma}{dE_c d\Omega_c d\Omega_n} = \frac{2\pi\mu_{pt}}{\hbar^2 K_i}\frac{1}{(2J_p+1)}\sum_{M_c\sigma M_p}|T_{M_c\sigma;M_p}|^2 \times \rho(E_c,\Omega_c,\Omega_n), \tag{10}$$

where $\rho(E_c,\Omega_c,\Omega_n)$ is the three-body phase space factor [29],

$$\rho(E_c,\Omega_c,\Omega_n) = \frac{m_c m_n \hbar k_c \hbar k_n}{(2\pi\hbar)^6} \times \left[\frac{m_t}{m_n + m_t + m_n(\mathbf{k}_c - \mathbf{K}_0)\cdot\mathbf{k}_n/k_n^2}\right]. \tag{11}$$

Here $\hbar\mathbf{K}_0$ is the total momentum of the system, and $\hbar\mathbf{k}_c$ and $\hbar\mathbf{k}_n$ are the momenta of the particles *c* and *n* in the final

state. Substituting Eq. (8) into Eq. (10) and carrying out the spin projection summations one gets

$$\frac{d^3\sigma}{dE_c d\Omega_c d\Omega_n} = \frac{2\pi\mu_{pt}}{\hbar^2 K_i} \sum_{jlm} \frac{S_{lj}}{(2l+1)} |B_{lm}|^2 \rho(E_c, \Omega_c, \Omega_n). \tag{12}$$

A. Approximations to the DWBA theory

The calculation of the reduced transition amplitudes B_{lm} is quite difficult task because a six-dimensional integration is involved. Therefore, different additional approximations have been used, such as the zero-range approximation (ZRA), e.g., Ref. [30], the Baur-Trautmann approximation (BTA) [31], or the local momentum approximation (LMA), e.g., Refs. [32–34]. These approximate methods provide a separation of the amplitude B_{lm} into two factors, each involving a three-dimensional integral.

1. Zero-range approximation

The ZRA is defined by [30]

$$V_{nc}(\mathbf{r})\Phi_p^{lm}(\mathbf{r}) = D_0 \delta(\mathbf{r}), \tag{13}$$

where D_0 is the usual zero-range constant,

$$D_0 = \int d\mathbf{r} V_{nc}(\mathbf{r})\Phi_p^{lm}(\mathbf{r}). \tag{14}$$

The effect of the ZRA is $\mathbf{r}_{ct} \to \mathbf{R}$, $\mathbf{R}_n \to \beta\mathbf{R}$, so that B_{lm} becomes a three-dimensional integral,

$$B_{lm}^{\mathrm{ZRA}} = D_0 \langle \chi^{(-)}(\mathbf{k}_{ct}, \mathbf{R}) e^{i\beta\mathbf{K}_n\cdot\mathbf{R}} | \chi^{(+)}(\mathbf{K}_i, \mathbf{R}) \rangle. \tag{15}$$

Thus, in the ZRA one assumes that the product of the three scattering waves in the integral in Eq. (9) is constant over the range of $V_{nc}(\mathbf{r})\Phi_p^{lm}(\mathbf{r})$. The approximation cannot be justified for higher energies and heavier projectiles [28,34]. Moreover, the ZRA implies that the c-t relative motion in the projectile has s state only.

2. Baur-Trautmann approximation

Baur and Trautmann [31] have proposed to replace the projectile-target relative coordinate $\mathbf{R}$ in the projectile distorted wave by the core-target relative coordinate $\mathbf{r}_{ct}$, i.e.,

$$\chi^{(+)}(\mathbf{K}_i, \mathbf{R}) \to \chi^{(+)}(\mathbf{K}_i, \mathbf{r}_{ct}). \tag{16}$$

With this approximation (BTA) the reduced amplitude separates in the following way:

$$B_{lm}^{\mathrm{BTA}} = \langle e^{i\mathbf{K}_n\cdot\mathbf{r}} | V_{nc}(\mathbf{r}) | \Phi_p^{lm}(\mathbf{r}) \rangle \times \langle \chi^{(-)}(\mathbf{k}_{ct}, \mathbf{r}_{ct}) e^{i\beta\mathbf{K}_n\cdot\mathbf{r}_{ct}} | \chi^{(+)}(\mathbf{K}_i, \mathbf{r}_{ct}) \rangle. \tag{17}$$

It has been argued [24,31] that through this approximation one takes into account, in a certain way, the fact that the projectile is polarized in the Coulomb field of the target nucleus. This approximation can also be looked upon as replacing the exact three-body wave function in Eq. (4) by the product $\Phi_{J_pM_p}(\xi_c, \xi_n, \mathbf{r})\chi^{(+)}(\mathbf{K}_i, \mathbf{r}_{ct})$.

3. Local momentum approximation

Another approximation scheme that leads to the factorization is the LMA [33,34]. The Coulomb distorted wave $\chi^{(+)}(\mathbf{K}_i, \mathbf{R})$ may be expanded about the point $\mathbf{r}_{ct}$,

$$\chi^{(+)}(\mathbf{K}_i, \mathbf{r}_{ct} + \alpha\mathbf{r}) = e^{\alpha\mathbf{r}\cdot\boldsymbol{\nabla}} \chi^{(+)}(\mathbf{K}_i, \mathbf{r}_{ct}), \tag{18}$$

where $\boldsymbol{\nabla}$ operates on the coordinate $\mathbf{r}_{ct}$. In the LMA the operator $-i\boldsymbol{\nabla}$ is replaced by the local momentum $\mathbf{K}_i'$ in the projectile-target potential $V_{pt}(R)$, evaluated at some representative distance R_0. This approximation provides a factorization of the reduced amplitude,

$$B_{lm}^{\mathrm{LMA}} = \langle e^{i[\mathbf{k} - \alpha(\mathbf{K}_i' - \mathbf{K}_f)]\cdot\mathbf{r}} | V_{nc}(\mathbf{r}) | \Phi_p^{lm}(\mathbf{r}) \rangle \times \langle \chi^{(-)}(\mathbf{k}_{ct}, \mathbf{r}_{ct}) e^{i\beta\mathbf{K}_n\cdot\mathbf{r}_{ct}} | \chi^{(+)}(\mathbf{K}_i, \mathbf{r}_{ct}) \rangle. \tag{19}$$

Similarly, applying the LMA to the final channel Coulomb distorted wave, i.e.,

$$\chi^{(-)}(\mathbf{k}_{ct}, \mathbf{R} - \alpha\mathbf{r}) \approx e^{-i\alpha\mathbf{k}_{ct}'\cdot\mathbf{r}} \chi^{(-)}(\mathbf{k}_{ct}, \mathbf{R}), \tag{20}$$

where $\mathbf{k}_{ct}'$ is the local momentum in the core-target potential $V_{ct}(r_{ct})$, one obtains the following factorized form of the reduced amplitude:

$$B_{lm}^{\mathrm{LMA}} = \langle e^{i[\mathbf{k} - \alpha(\mathbf{k}_{ct}' - \mathbf{k}_{ct})]\cdot\mathbf{r}} | V_{nc}(\mathbf{r}) | \Phi_p^{lm}(\mathbf{r}) \rangle \times \langle \chi^{(-)}(\mathbf{k}_{ct}, \mathbf{R}) e^{i\beta\mathbf{K}_n\cdot\mathbf{R}} | \chi^{(+)}(\mathbf{K}_i, \mathbf{R}) \rangle. \tag{21}$$

The validity of the LMA and the choice of the magnitude and direction of the local momentum are discussed in Refs. [25,26]. In the following, the LMA amplitudes of Eqs. (19) and (21) will be referred to as the ILMA (initial channel LMA) and FLMA (final channel LMA) amplitudes, respectively.

4. Asymptotic momentum approximation

The distorted wave function $\chi^{(+)}(\mathbf{K}_i, \mathbf{R})$ can be written in the form

$$\chi^{(+)}(\mathbf{K}_i, \mathbf{R}) = e^{i\mathbf{K}_i\cdot\mathbf{R}} D^{(+)}(\mathbf{K}_i, \mathbf{R}), \tag{22}$$

where $D^{(+)}(\mathbf{K}_i, \mathbf{R})$ is a distortion function. Assuming that the distortion function does not change significantly over the range of $V_{nc}(\mathbf{r})\Phi_p^{lm}(\mathbf{r})$, we can write

$$\begin{aligned} \chi^{(+)}(\mathbf{K}_i, \mathbf{R}) &= e^{i\mathbf{K}_i\cdot(\mathbf{r}_{ct} + \alpha\mathbf{r})} D^{(+)}(\mathbf{K}_i, \mathbf{r}_{ct} + \alpha\mathbf{r}) \\ &\approx e^{i\mathbf{K}_i\cdot(\mathbf{r}_{ct} + \alpha\mathbf{r})} D^{(+)}(\mathbf{K}_i, \mathbf{r}_{ct}) \\ &= e^{i\alpha\mathbf{K}_i\cdot\mathbf{r}} \chi^{(+)}(\mathbf{K}_i, \mathbf{r}_{ct}). \end{aligned} \tag{23}$$

Substituting Eq. (23) into Eq. (9) gives

$$B_{lm}^{\mathrm{AMA}} = \langle e^{i[\mathbf{k} - \alpha(\mathbf{K}_i - \mathbf{K}_f)]\cdot\mathbf{r}} | V_{nc}(\mathbf{r}) | \Phi_p^{lm}(\mathbf{r}) \rangle \times \langle \chi^{(-)}(\mathbf{k}_{ct}, \mathbf{r}_{ct}) e^{i\beta\mathbf{K}_n\cdot\mathbf{r}_{ct}} | \chi^{(+)}(\mathbf{K}_i, \mathbf{r}_{ct}) \rangle. \tag{24}$$

TABLE I. Abbreviations used in the text for various approximations to the distorted-wave Born approximation (DWBA).

Abbreviation	Explanation
ZRA	Zero-range approximation
BTA	Approximation of Baur and Trautmann
LMA	Local momentum approximation
ILMA	Local momentum approximation to the distorted wave in the initial channel
FLMA	Local momentum approximation to the distorted wave in the final channel
AMA	Asymptotic momentum approximation
IAMA	Asymptotic momentum approximation to the distorted wave in the initial channel
FAMA	Asymptotic momentum approximation to the distorted wave in the final channel
EDWBA	Exact distorted-wave Born approximation

Similarly, assuming that the distorted wave function for the exit channel can be approximated as

$$\chi^{(-)*}(\mathbf{k}_{ct},\mathbf{r}_{ct}) = e^{-i\mathbf{k}_{ct}\cdot(\mathbf{R}-\alpha\mathbf{r})} D^{(-)*}(\mathbf{k}_{ct},\mathbf{R}-\alpha\mathbf{r}) \approx e^{-i\mathbf{k}_{ct}\cdot(\mathbf{R}-\alpha\mathbf{r})} D^{(-)*}(\mathbf{k}_{ct},\mathbf{R}) = e^{i\alpha\mathbf{k}_{ct}\cdot\mathbf{r}} \chi^{(-)*}(\mathbf{k}_{ct},\mathbf{R}), \quad (25)$$

the transition amplitude becomes

$$B_{lm}^{\mathrm{AMA}} = \langle e^{i\mathbf{k}\cdot\mathbf{r}} | V_{nc}(\mathbf{r}) | \Phi_p^{lm}(\mathbf{r}) \rangle \times \langle \chi^{(-)}(\mathbf{k}_{ct},\mathbf{R}) e^{i\beta\mathbf{K}_n\cdot\mathbf{R}} | \chi^{(+)}(\mathbf{K}_i,\mathbf{R}) \rangle. \quad (26)$$

Similar approximation to distortion function has been used in a distorted-wave description of knockout reactions, e.g., Ref. [35]. Equations (24) and (26) can also be obtained in the LMA by replacing the local momenta $\mathbf{K}_i'$ and $\mathbf{k}_{ct}'$ in Eqs. (19) and (21) by their asymptotic values $\mathbf{K}_i$ and $\mathbf{k}_{ct}$. It may be noted that the approximate amplitude (24) is identical to the amplitude recently derived within the adiabatic model of the Coulomb breakup reactions [28]. However, the underlying physical picture is different [25]. In the following, the asymptotic momentum approximation (AMA) amplitudes of Eqs. (24) and (26) will be referred to as the IAMA (initial channel AMA) and FAMA (final channel AMA) amplitudes, respectively.

Abbreviations used in this paper for different approximations to the DWBA breakup amplitude are explained in Table I.

B. Evaluation of the approximate transition amplitude

The common result of all these approximation schemes is that the transition amplitude separates in the following way:

$$B_{lm} \approx \langle e^{i\mathbf{q}_{nc}\cdot\mathbf{r}} | V_{nc}(\mathbf{r}) | \Phi_p^{lm}(\mathbf{r}) \rangle \times \langle \chi^{(-)}(\mathbf{k}_{ct},\mathbf{r}') e^{i\beta\mathbf{K}_n\cdot\mathbf{r}'} | \chi^{(+)}(\mathbf{K}_i,\mathbf{r}') \rangle. \quad (27)$$

The first factor in this equation is the so called vertex function and it involves the information about the internal structure of the projectile. It can be expressed as

$$\langle e^{i\mathbf{q}_{nc}\cdot\mathbf{r}} | V_{nc}(\mathbf{r}) | \Phi_p^{lm}(\mathbf{r}) \rangle = F(\mathbf{q}_{nc}) = F_l(q_{nc}) Y_{lm}(\hat{\mathbf{q}}_{nc}), \quad (28)$$

where

$$F_l(q_{nc}) = 4\pi \int dr r^2 j_l(q_{nc} r) V_{nc}(r) u_l(r). \quad (29)$$

The amplitudes of Eqs. (15), (17), (19), (21), (24), and (26) differ only through the momenta $\mathbf{q}_{nc}$ that appear in the vertex function $F(\mathbf{q}_{nc})$. The expressions for these momenta are summarized in Table II.

The second term in Eq. (27) contains the dynamics of the breakup process. The same type of integral appears in the calculations of the bremsstrahlung cross sections where it has been expressed in terms of hypergeometric functions [36,37]. Using the following expressions for the Coulomb distorted waves in the initial and final channel:

TABLE II. Momenta $\mathbf{q}_{nc}$ which appear in the vertex function $F(\mathbf{q}_{nc})$ for different approximation methods: the zero-range approximation (ZRA), the Baur-Trautmann approximation (BTA), the local momentum approximations (ILMA and FLMA), and the asymptotic momentum approximations (IAMA and FAMA).

ZRA	BTA	ILMA	FLMA	IAMA	FAMA
0	$\mathbf{k}+\alpha\mathbf{K}_f$	$\mathbf{k}-\alpha(\mathbf{K}_i'-\mathbf{K}_f)$	$\mathbf{k}-\alpha(\mathbf{k}_{ct}'-\mathbf{k}_{ct})$	$\mathbf{k}-\alpha(\mathbf{K}_i-\mathbf{K}_f)$	$\mathbf{k}$

$$\chi^{(+)}(\mathbf{K}_i,\mathbf{R})=e^{-\pi\eta_{pt}/2}\Gamma(1+i\eta_{pt})e^{i\mathbf{K}_i\cdot\mathbf{R}}{}_1F_1[-i\eta_{pt},1;i(K_iR-\mathbf{K}_i\cdot\mathbf{R})], \tag{30}$$

$$\chi^{(-)*}(\mathbf{k}_{ct},\mathbf{r}_{ct})=e^{-\pi\eta_{ct}/2}\Gamma(1+i\eta_{ct})e^{-i\mathbf{k}_{ct}\cdot\mathbf{r}_{ct}}{}_1F_1[-i\eta_{ct},1;i(k_{ct}r_{ct}+\mathbf{k}_{ct}\cdot\mathbf{r}_{ct})], \tag{31}$$

one obtains for the second factor

$$\langle\chi^{(-)}(\mathbf{k}_{ct},\mathbf{r}')e^{i\beta\mathbf{K}_n\cdot\mathbf{r}'}|\chi^{(+)}(\mathbf{K}_i,\mathbf{r}')\rangle=e^{-\pi(\eta_{pt}+\eta_{ct})/2}\Gamma(1+i\eta_{pt})\Gamma(1+i\eta_{ct})I. \tag{32}$$

In this equation I is the bremsstrahlung integral given by [37,38]

$$I=-\lim_{\varepsilon\to0}\frac{d}{d\varepsilon}\{A(\varepsilon)\,{}_2F_1[-i\eta_{pt},-i\eta_{ct};1;z(\varepsilon)]\}, \tag{33}$$

where

$$A(\varepsilon)=\frac{4\pi}{(Q^2+\varepsilon^2)^{1+i\eta_{pt}+i\eta_{ct}}}(Q^2+\varepsilon^2-2\mathbf{Q}\cdot\mathbf{K}_i-2i\varepsilon K_i)^{i\eta_{pt}}(Q^2+\varepsilon^2+2\mathbf{Q}\cdot\mathbf{k}_{ct}-2i\varepsilon k_{ct})^{i\eta_{ct}}, \tag{34}$$

$$z(\varepsilon)=\frac{2(Q^2+\varepsilon^2)(K_ik_{ct}+\mathbf{K}_i\cdot\mathbf{k}_{ct})-4(\mathbf{Q}\cdot\mathbf{K}_i+i\varepsilon K_i)(\mathbf{Q}\cdot\mathbf{k}_{ct}-i\varepsilon k_{ct})}{(Q^2+\varepsilon^2-2\mathbf{Q}\cdot\mathbf{K}_i-2i\varepsilon K_i)(Q^2+\varepsilon^2+2\mathbf{Q}\cdot\mathbf{k}_{ct}-2i\varepsilon k_{ct})}, \tag{35}$$

with

$$\mathbf{Q}=\mathbf{K}_i-\mathbf{k}_{ct}-\beta\mathbf{K}_n=\mathbf{K}_i-\mathbf{K}_f. \tag{36}$$

Here ε is a real positive parameter. In Eqs. (30)–(34) η_{pt} and η_{ct} are the Coulomb parameters,

$$\eta_{pt}=\frac{Z_pZ_te^2\mu_{pt}}{\hbar^2K_i},\qquad \eta_{ct}=\frac{Z_cZ_te^2\mu_{ct}}{\hbar^2k_{ct}}, \tag{37}$$

where μ_{pt} and μ_{ct} are the reduced masses in the corresponding channels.

C. Transition amplitude in momentum space

The reduced amplitude of Eq. (9) can be expressed in terms of momentum wave functions as a three-dimensional integral. The Fourier transform of a Coulomb wave function $\chi^{(+)}(\mathbf{k}_{ij},\mathbf{r}_{ij})$ is defined by

$$\phi^{(+)}(\mathbf{k}_{ij},\mathbf{q}_{ij})=\int d\mathbf{r}_{ij}e^{-i\mathbf{q}_{ij}\cdot\mathbf{r}_{ij}}\chi^{(+)}(\mathbf{k}_{ij},\mathbf{r}_{ij}), \tag{38}$$

$$\chi^{(+)}(\mathbf{k}_{ij},\mathbf{r}_{ij})=\frac{1}{(2\pi)^3}\int d\mathbf{q}_{ij}e^{i\mathbf{q}_{ij}\cdot\mathbf{r}_{ij}}\phi^{(+)}(\mathbf{k}_{ij},\mathbf{q}_{ij}). \tag{39}$$

Using the Fourier representations of the Coulomb wave functions of Eqs. (30) and (31) the reduced amplitude can be written as

$$B_{lm}=\frac{1}{(2\pi)^3}\int d\mathbf{Q}_iF[\mathbf{k}-\alpha(\mathbf{Q}_i-\mathbf{K}_f)]\times\phi^{(-)*}(\mathbf{k}_{ct},\mathbf{Q}_i-\mathbf{K}_f+\mathbf{k}_{ct})\phi^{(+)}(\mathbf{K}_i,\mathbf{Q}_i), \tag{40}$$

where $F(\mathbf{q})$, $\mathbf{q}=\mathbf{k}-\alpha(\mathbf{Q}_i-\mathbf{K}_f)$, is the vertex function defined by Eq. (28). We note that the vertex function now appears within the integrand while it enters as a multiplicative factor in Eq. (27) for the approximate DWBA amplitude.

The Coulomb wave in momentum space was derived by Guth and Mullin [39],

$$\phi^{(+)}(\mathbf{k}_{ij},\mathbf{q}_{ij})=-4\pi e^{-\pi\eta_{ij}/2}\Gamma(1+i\eta_{ij})\times\lim_{\varepsilon\to0}\frac{d}{d\varepsilon}\left\{\frac{[q_{ij}^2-(k_{ij}+i\varepsilon)^2]^{i\eta_{ij}}}{[|\mathbf{q}_{ij}-\mathbf{k}_{ij}|^2+\varepsilon^2]^{1+i\eta_{ij}}}\right\}. \tag{41}$$

It can be expressed as

$$\phi^{(+)}(\mathbf{k}_{ij},\mathbf{q}_{ij})=\varphi^{(+)}(\mathbf{k}_{ij},\mathbf{q}_{ij})-8\pi\eta_{ij}k_{ij}e^{-\pi\eta_{ij}/2}\Gamma(1+i\eta_{ij})\times\lim_{\varepsilon\to0}\left\{\frac{[q_{ij}^2-(k_{ij}+i\varepsilon)^2]^{-1+i\eta_{ij}}}{[|\mathbf{q}_{ij}-\mathbf{k}_{ij}|^2+\varepsilon^2]^{1+i\eta_{ij}}}\right\}. \tag{42}$$

Here the first term is the Coulomb asymptotic state in the momentum representation [40]. It is a δ-function-type term with support at the point $\mathbf{q}_{ij}=\mathbf{k}_{ij}$.

1. Factorization approximation

We now assume that the dominant contribution to the integral in Eq. (40) comes from the region around a point $\mathbf{Q}_i=\mathbf{Q}_i^0$ and that the vertex function $F(\mathbf{q})$ is the slowly varying function of $\mathbf{Q}_i$ so that it can be factored out of the integral at the point $\mathbf{q}_{nc}=\mathbf{k}-\alpha(\mathbf{Q}_i^0-\mathbf{K}_f)$. The transition amplitude then reads

$$B_{lm} \approx B^0_{lm} = F[\mathbf{k} - \alpha(\mathbf{Q}^0_i - \mathbf{K}_f)] \frac{1}{(2\pi)^3} \int d\mathbf{Q}_i \times \phi^{(-)*}(\mathbf{k}_{ct}, \mathbf{Q}_i - \mathbf{K}_f + \mathbf{k}_{ct}) \phi^{(+)}(\mathbf{K}_i, \mathbf{Q}_i) = F(\mathbf{q}_{nc}) \langle \chi^{(-)}(\mathbf{k}_{ct}, \mathbf{R}) e^{i\beta \mathbf{K}_n \cdot \mathbf{R}} | \chi^{(+)}(\mathbf{K}_i, \mathbf{R}) \rangle. \quad (43)$$

The exact transition amplitude can be rewritten as

$$B_{lm} = B^0_{lm} + \Delta B_{lm}, \quad (44)$$

where

$$\Delta B_{lm} = \frac{1}{(2\pi)^3} \int d\mathbf{Q}_i \{ F[\mathbf{k} - \alpha(\mathbf{Q}_i - \mathbf{K}_f)] - F[\mathbf{k} - \alpha(\mathbf{Q}^0_i - \mathbf{K}_f)] \} \times \phi^{(-)*}(\mathbf{k}_{ct}, \mathbf{Q}_i - \mathbf{K}_f + \mathbf{k}_{ct}) \phi^{(+)}(\mathbf{K}_i, \mathbf{Q}_i). \quad (45)$$

If the Coulomb distortion is weak, then the Coulomb distorted waves $\phi^{(+)}(\mathbf{K}_i, \mathbf{Q}_i)$ and $\phi^{(-)*}(\mathbf{k}_{ct}, \mathbf{Q}_i - \mathbf{K}_f + \mathbf{k}_{ct})$ in Eq. (40) are sharply peaked at $\mathbf{Q}_i = \mathbf{K}_i$ and $\mathbf{Q}_i = \mathbf{K}_f$, respectively. Consequently, we assume that the most important contributions to the integral in Eq. (40) come from the regions around these two points. If we choose $\mathbf{Q}^0_i = \mathbf{K}_i$ in Eq. (43), then $\mathbf{q}_{nc} = \mathbf{k} - \alpha(\mathbf{K}_i - \mathbf{K}_f)$, and we obtain the IAMA amplitude of Eq. (24). Alternatively, if we approximate $\mathbf{Q}^0_i$ by $\mathbf{K}_f$ in Eq. (43), then $\mathbf{q}_{nc} = \mathbf{k}$, and we obtain the FAMA amplitude of Eq. (26). Similarly, if we choose for $\mathbf{Q}^0_i$ the value corresponding to an effective momentum in the entrance channel ($\mathbf{K}'_i$), or in the exit channel ($\mathbf{k}'_{ct}$), for which the integrand in Eq. (40) is large, we obtain the ILMA and FLMA amplitudes of Eqs. (19) and (21), respectively. In general, the ZRA and BTA cannot be obtained from Eq. (43) with a reasonable choice of $\mathbf{Q}^0_i$. The ZRA is equivalent to the $\alpha \mathbf{Q}^0_i = \mathbf{k} + \alpha \mathbf{K}_f$ approximation and the BTA corresponds to the $\alpha \mathbf{Q}^0_i = 0$ approximation to Eq. (43).

Thus, the approximations which lead to the amplitudes of Eqs. (15), (17), (19), (21), (24), and (26) are equivalent to the assumption that the vertex function $F(\mathbf{q})$ in Eq. (40) can be replaced by the value given by the effective momentum $\mathbf{q}_{nc}$ specified in Table II. Numerical tests of the accuracy of these approximations are presented in the following section.

III. NUMERICAL RESULTS

In this section the results of calculations with different approximate DWBA methods are compared with those obtained with the exact DWBA (EDWBA). The calculations of the exact DWBA transition amplitude was performed by using Eqs. (43)–(45). The approximate amplitude B^0_{lm} in Eq. (44) was calculated within the ZRA or FAMA model. After a suitable transformation of the integral in Eq. (45) the integration was carried out numerically using the computer code DCUHRE [41]. The procedure of integration will be described in more detail elsewhere.

The triple differential cross sections were calculated for the deuteron breakup on ^{12}C and ^{208}Pb nuclei at the deuteron energy of 140 MeV, and for the ^{11}Be breakup on ^{208}Pb at the beam energy of 72 MeV/nucleon, for very forward angles. Localization of these breakup processes in momentum, which enters the vertex function was investigated numerically. The results are analyzed and the validity of the factorization approximation is discussed.

The deuteron breakup reaction was chosen because the deuteron is a representative example of a weakly bound two-body system with a charged core and a neutral valence particle. It has been shown [28] that the DWBA with the BTA underestimates the (d,pn) breakup cross sections at beam energies $\gtrsim$30 MeV/nucleon. Furthermore, it has been argued [28] that the zero-range approximation to the DWBA breakup amplitude cannot be justified for these energies, either in the case of the (d,pn) reaction or for halo nuclei. The Coulomb breakup of the one-neutron halo nucleus ^{11}Be has been studied within the local momentum approximations to the DWBA, ILMA [25], and FLMA [26], as well as within the BTA [26]. The ILMA and FLMA gave results that are similar to those obtained within the adiabatic breakup theory, and consistent with experimental data [25,26] while the BTA failed to explain the data [26].

A. The (d,pn) reaction

The triple differential cross sections $d^3\sigma/dE_p d\Omega_p d\Omega_n$ were calculated as a function of the proton energy E_p, for several pairs of very forward angles θ_p and θ_n. [In this

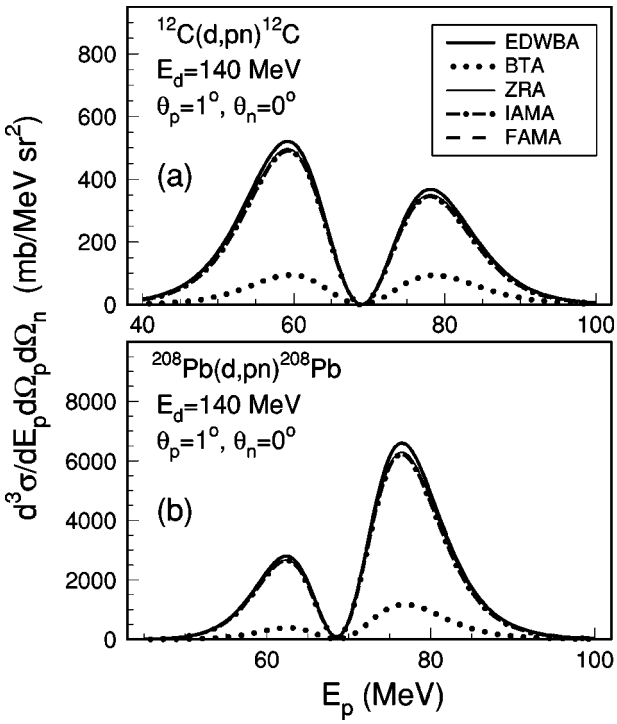

FIG. 2. Triple differential cross sections as a function of the proton energy E_p for the (d,pn) breakup at $E_d = 140$ MeV, $\theta_p = 1°$, and $\theta_n = 0°$, (a) on a ^{12}C target and (b) on a ^{208}Pb target. The curves represent the EDWBA (thick solid), the BTA (dotted), the ZRA (thin solid), the IAMA (thick dash dotted), and the FAMA (thick dashed) calculations.

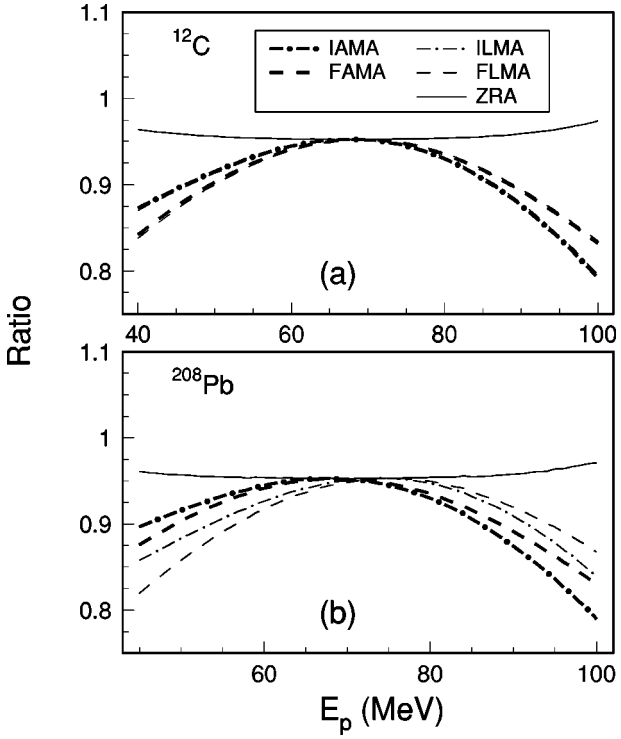

FIG. 3. Ratios of the approximate to the exact DWBA cross sections as a function of the proton energy E_p for the (d,pn) breakup at $E_d=140$ MeV, $\theta_p=1°$, and $\theta_n=0°$, (a) on a ^{12}C target and (b) on a ^{208}Pb target. The curves compare the IAMA (thick dash dotted), the FAMA (thick dashed), the ILMA (thin dash dotted), the FLMA (thin dashed), and the ZRA (thin solid) results.

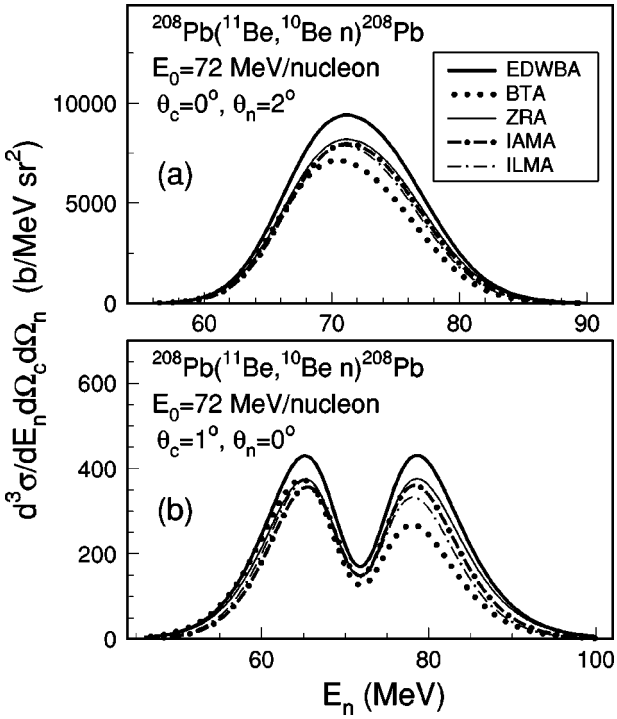

FIG. 4. Triple differential cross sections as a function of the neutron energy E_n for the ^{208}Pb(^{11}Be,^{10}Be n)^{208}Pb reaction at the beam energy $E_0=72$ MeV/nucleon, (a) at $\theta_c=0°$ and $\theta_n=2°$, and (b) at $\theta_c=1°$ and $\theta_n=0°$. The curves compare the exact DWBA (thick solid), the BTA (dotted), the ZRA (thin solid), the IAMA (thick dash dotted), and the ILMA (thin dash dotted) results.

section, in the case of the (d,pn) reaction, the projectile, core, and valence particle are denoted by d (deuteron), p (proton), and n (neutron), respectively.] The calculations were performed using the Hulthén vertex function given explicitly in Ref. [31]. The local momenta $\mathbf{K}_i'$ and $\mathbf{k}_{ct}'$, used in the ILMA and FLMA calculations, were evaluated at 10 fm with the directions being the same as those of the asymptotic momenta $\mathbf{K}_i$ and $\mathbf{k}_{ct}$, respectively.

Figure 2 shows the cross sections for ^{12}C and ^{208}Pb targets at $E_d=140$ MeV, $\theta_p=1°$, and $\theta_n=0°$. The thick curves show the breakup cross sections calculated using the EDWBA amplitude. The results obtained within the approximate DWBA methods are represented by the thin curves (ZRA), thick dash-dotted curves (IAMA), thick dashed curves (FAMA), and dotted curves (BTA). It can be noted that the results of the ZRA and AMA methods are close to the results obtained with the exact DWBA while the BTA underestimates them considerably. The effects of the zero-range and asymptotic momentum approximations to the DWBA in the energy integrated cross sections are 5% and 6–7 %, respectively, for both targets. The results of the LMA calculations (not shown in this figure) are similar to those of the AMA.

The ratios of the ZRA, LMA, and AMA to the EDWBA cross sections are shown in Fig. 3 as a function of the proton energy. We observe that the IAMA (ILMA) and FAMA (FLMA) results are close to each other and that the ZRA method yields the best overall agreement with the EDWBA calculations. In the ^{12}C case, the results of the IAMA and FAMA are nearly identical to the results of ILMA and FLMA, respectively. Similar results are obtained for the other angles studied.

B. ^{208}Pb(^{11}Be,^{10}Be n)^{208}Pb reaction

The bound state of the ^{11}Be was assumed to have a $2s_{1/2}$ neutron coupled to the 0^+ ^{10}Be core with a binding energy of 504 keV. The corresponding single particle wave function was calculated from a Woods-Saxon potential with radius and diffuseness parameters 1.15 fm and 0.5 fm, respectively. The depth of the potential was adjusted to reproduce the binding energy. The spectroscopic factor was set to unity throughout the calculations.

The triple differential cross sections were calculated as a function of the neutron energy for a few pairs of forward angles of the outgoing particles. The results for $\theta_c=0°$, $\theta_n=2°$, and $\theta_c=1°$, $\theta_n=0°$ are presented in Fig. 4. The local momenta $\mathbf{K}_i'$ and $\mathbf{k}_{ct}'$, used in the LMA calculations, were evaluated in the same way as for the (d,pn) reaction. The results of the FLMA and FAMA (not shown in this figure) are almost identical to the results of the ILMA and IAMA, respectively.

Figure 5 shows the ratios of the approximate to the EDWBA cross sections as a function of the neutron energy E_n, for the same angles as in Fig. 4. We can see that the errors of the approximate DWBA models can be significant. Again,

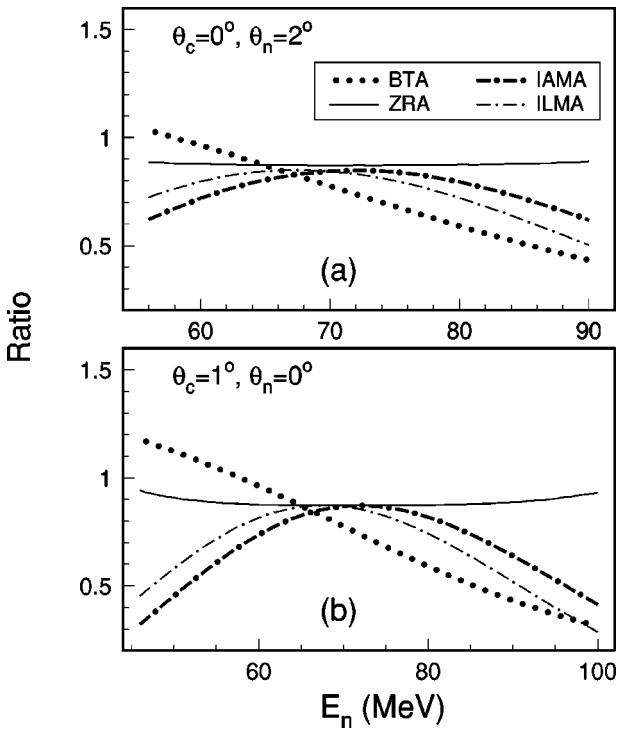

FIG. 5. Ratios of the approximate to the exact DWBA cross sections as a function of E_n for the ^{208}Pb(^{11}Be,^{10}Be n)^{208}Pb reaction at $E_0=72$ MeV/nucleon, (a) at $\theta_c=0°$ and $\theta_n=2°$, and (b) at $\theta_c=1°$ and $\theta_n=0°$. The curves compare the BTA (dotted), the ZRA (thin solid), the IAMA (thick dash dotted), and the ILMA (thin dash dotted) calculations.

the ZRA reproduces the shape and magnitude of the ED-WBA triple differential cross sections better than the other models. The effect of the ZRA in the energy integrated cross sections is ~12%, while the effects of the AMA and LMA are ~20%, and that of the BTA is ~27%.

C. Validity of the factorization approximation

In order to clarify these results, calculations were performed to investigate the localization of the DWBA amplitude in momentum q which enters the vertex function $F_0(q)$. To this end the following quantities have been introduced:

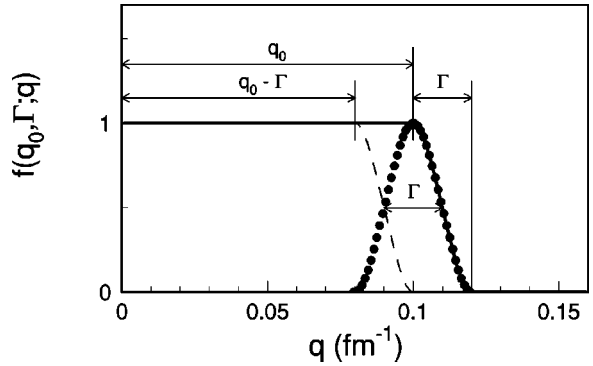

FIG. 6. Cutoff function $f(q_0,\Gamma;q)$ used in test calculations of the ratios $R(q_0)$ (solid curve) and $\Delta R(q_0)$ (dotted curve), as a function of q, with $q_0=0.1$ fm^{-1} and $\Gamma=0.02$ fm^{-1}.

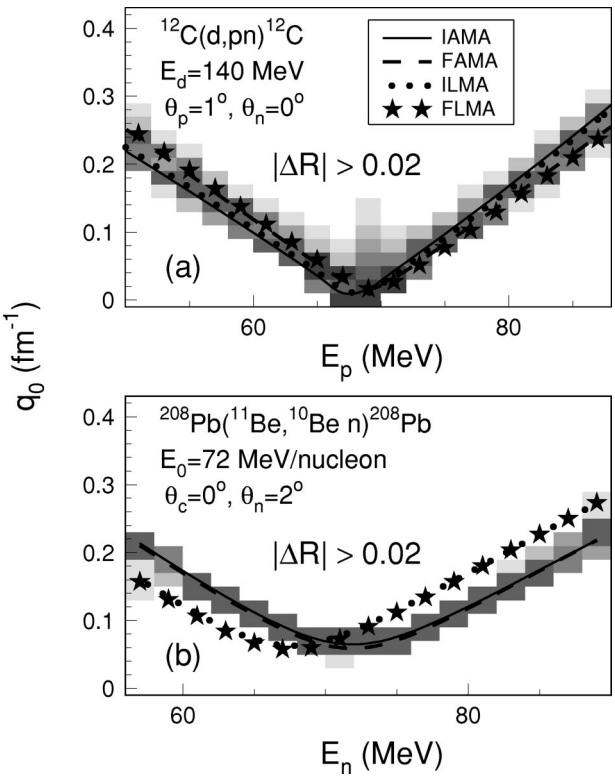

FIG. 7. Localization in q of the contributions to the transition amplitude. (a) Ratios $|\Delta R(q_0)|$ as a function of the momentum q_0 and proton energy E_p for the ^{12}C(d,pn)^{12}C reaction at $\theta_p=1°$ and $\theta_n=0°$. (b) Ratios $|\Delta R(q_0)|$ as a function of the momentum q_0 and neutron energy E_n for the ^{208}Pb(^{11}Be,^{10}Be n)^{208}Pb reaction at $\theta_c=0°$ and $\theta_n=2°$. The calculations use $\Gamma=0.02$ fm^{-1}. Also shown are the momenta q_{nc} relevant to the approximate models: IAMA (solid curves), FAMA (dashed curves), ILMA (dotted curves), and FLMA (stars).

$$R(q_0)=\frac{B_{00}^{q_0}}{B_{00}} \tag{46}$$

and

$$\Delta R(q_0)=R(q_0)-R(q_0-\Gamma)=\frac{\Delta B_{00}^{q_0}}{B_{00}}. \tag{47}$$

Here $B_{00}^{q_0}$ denotes the transition amplitude obtained by multiplying the integrand in Eq. (40) by the near-rectangular cutoff function $f(q_o,\Gamma;q)$, shown by the solid curve in Fig. 6, where Γ is the width of the smooth cutoff region. The amplitude $\Delta B_{00}^{q_0}$ corresponds to the cutoff function shown by the dotted curve in Fig. 6. If the contribution to the transition amplitude comes from a region $q_a \leqslant q \leqslant q_b$, then $R(q_0)=0$ for $q_0<q_a-\Gamma$, $R(q_0)=1$ for $q_0>q_b$, and $\Delta R(q_0)=0$ for $q_0<q_a-\Gamma$ or $q_0>q_b+\Gamma$. Thus, the ratio $\Delta R(q_0)$ is a measure of the contribution to the transition amplitude in the region $q\sim q_0$.

Figure 7 shows the ratios $|\Delta R(q_0)|$, with $\Gamma=0.02$ fm^{-1}, (a) for the case of the ^{12}C(d,pn)^{12}C reaction, as a function of q_0 and the energy E_p, and (b) for the case of the

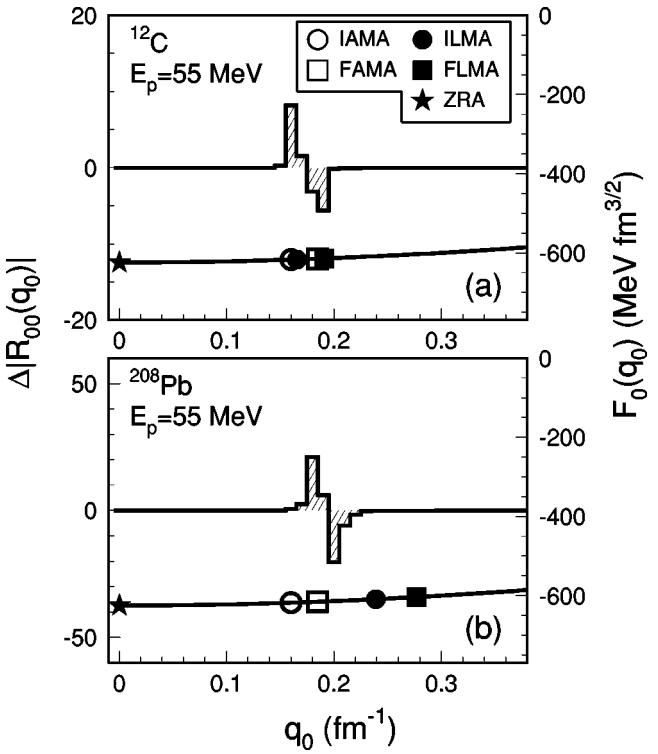

FIG. 8. Histograms of $\Delta|R(q_0)|$, using $\Gamma=0.01$ fm^{-1}, for the deuteron breakup process at $\theta_p=1°$ and $\theta_n=0°$, for $E_p=55$ MeV, (a) on ^{12}C and (b) on ^{208}Pb. Also presented (solid curves) is the vertex function $F_0(q_0)$ calculated for the Hulthén deuteron wave function. The symbols show the momenta q_{nc} probed by the approximate transition amplitudes.

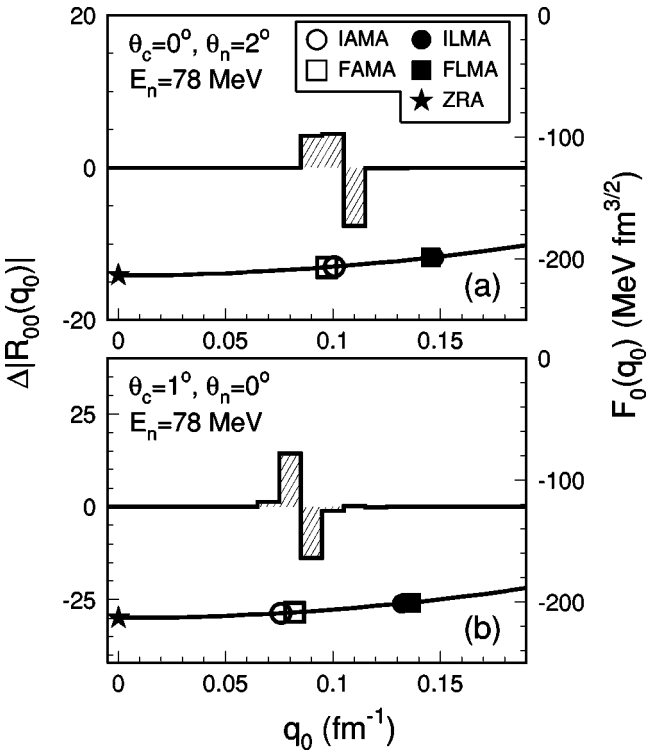

FIG. 9. Histograms of $\Delta|R(q_0)|$, using $\Gamma=0.01$ fm^{-1}, for the ^{11}Be breakup on ^{208}Pb, for $E_n=78$ MeV, (a) at $\theta_c=0°$ and $\theta_n=1°$, and (b) at $\theta_c=1°$ and $\theta_n=0°$. The solid curves represent the vertex function $F_0(q_0)$ for ^{11}Be. The symbols show the momenta q_{nc} probed by the approximate transition amplitudes.

^{208}Pb(^{11}Be,^{10}Be n)^{208}Pb reaction, as a function of q_0 and the energy E_n. We see that for a given energy E_p (E_n) the contributions to the the transition amplitude come mostly from a narrow range of momenta q. This reflects the localization of the integrand in Eq. (40) in momentum $\mathbf{Q}_i$. Also shown in this figure are the momenta q_{nc} that enter the vertex function in the AMA and LMA models. The momenta corresponding to the BTA are relatively large, ~ 1–2 fm^{-1} for the deuteron case and ~ 1.5–2.0 fm^{-1} for the ^{11}Be case. In the ZRA the vertex function is evaluated at $q_{nc}=0$. We observe that the dominant contributions to the DWBA amplitude come from the region around the momenta q_{nc} relevant to the AMA models.

Figures 8 and 9 illustrate the localization in q of the deuteron breakup reaction for $E_p=55$ MeV, and of the ^{11}Be breakup reaction for $E_n=78$ MeV, respectively. Histograms show the contributions $\Delta|R(q_0)|=|R(q_0)|-|R(q_0-\Gamma)|$, with $\Gamma=0.01$ fm^{-1}, as a function of q_0. Also shown are the vertex functions $F_0(q_0)$ (solid curves) and the momenta q_{nc} which enter the approximate transition amplitudes (symbols). We see in these two figures that the values of $F_0(q)$ sampled by the exact transition amplitude come from the neighborhood of the values relevant to the AMA models. However, it appears that the exact DWBA results are closer to the ZRA predictions, for which the absolute value of the vertex function is larger than that for the AMA models. This means that the factorization of the vertex function $F(\mathbf{q})$ out of the integral in Eq. (40), at a point from the region yielding dominant contributions to the integral, can lead to a poor approximation. Also evident in these figures is a strong interference in the momentum region contributing to the breakup amplitude. Thus, one may expect a significant sensitivity of the breakup amplitude to the nonconstancy of the vertex function in this region.

In the application of the FLMA model to the Coulomb breakup of neutron rich nuclei, e.g., Refs. [26,27], the magnitude of the local momentum $\mathbf{k}'_{ct}$ has been evaluated at 10 fm. The direction of $\mathbf{k}'_{ct}$ has been taken to be the same as that of the asymptotic momentum $\mathbf{k}_{ct}$. In this paper, the local momenta $\mathbf{K}'_i$ and $\mathbf{k}'_{ct}$ are evaluated in the same way. We can see from Figs. 7, 8, and 9 that this choice of the local momenta is not generally justified. In the ^{12}C case (low Z_t), it leads to the momenta q_{nc} almost identical to those corresponding to the asymptotic momenta. On the other hand, in the case of ^{208}Pb, for both reactions, the momenta q_{nc} corresponding to the AMA appear to be a better approximation to the momenta q which contribute to the process.

IV. SUMMARY AND CONCLUSIONS

In this paper, we have studied the validity of different approximations to the postform DWBA transition amplitude for the Coulomb breakup of neutron halo nuclei. Test calculations were performed within commonly used approximate

DWBA models as well as within the exact DWBA. The exact DWBA breakup amplitude is expressed in momentum space as a three-dimensional integral and evaluated numerically.

Triple differential cross sections were calculated for the Coulomb breakup of deuteron on ^{12}C and ^{208}Pb, and of ^{11}Be on ^{208}Pb, at the beam energy of $\sim$70 MeV/nucleon, for very forward angles. For both reactions the BTA cross sections deviate from the exact DWBA calculations most strongly. Qualitatively, the results of the ZRA, AMA, and LMA models for the (d,pn) reaction are similar to those for the ^{11}Be breakup reaction. In the case of the (d,pn) reaction, the results of these models for the energy integrated cross section differ from the exact DWBA calculations by $\sim$5–7 %. In the case of the ^{11}Be breakup reaction, the differences between the exact and approximate DWBA models are larger, $\sim$12% for the ZRA and $\sim$20% for the AMA and LMA. The results of the LMA and AMA models are similar to each other. For both reaction the ZRA gives the breakup cross sections closest in shape and magnitude to those calculated with the exact DWBA.

The localization of the transition amplitude in momentum which enters the vertex function has been studied. It appears that the dominant contributions to the breakup processes come from the neighborhood of the asymptotic momenta q_{nc}, relevant to the AMA models. However, these contributions interfere destructively and the resulting transition amplitude can be very sensitive to the behavior of the vertex function in the region around these momenta. Consequently, the factorization of the vertex function out of the integral at a point from the region yielding the dominant contributions to the process can lead to a significant error. This is the case for the AMA and LMA models. In the case of the LMA models, there is also uncertainty regarding the choice of the effective local momentum. The ZRA and BTA cannot be justified even in the case that the factorization approximation works. The relative success of the ZRA in the present calculations appears to be a numerical coincidence.

In conclusion, the present calculations show that the commonly used approximations to the DWBA amplitude for the Coulomb breakup of neutron halo nuclei are very suspecting. Since the numerical evaluation of the exact DWBA amplitude is rather time consuming, it is desirable to find approximations that reduce the computational complexity.

[1] K. Riisager, Rev. Mod. Phys. **66**, 1105 (1994).
[2] P.G. Hansen, A.S. Jensen, and B. Jonson, Annu. Rev. Nucl. Part. Sci. **45**, 591 (1995).
[3] I. Tanihata, J. Phys. G **22**, 157 (1996).
[4] I. Tanihata, T. Kobayashi, O. Yamakawa, S. Shimoura, K. Ekuni, K. Sugimoto, N. Takahashi, T. Shimoda, and H. Sato, Phys. Lett. B **206**, 592 (1988).
[5] M. Fukuda *et al.*, Phys. Lett. B **268**, 339 (1991).
[6] T. Kobayashi *et al.*, Phys. Lett. B **232**, 51 (1989).
[7] D. Sackett *et al.*, Phys. Rev. C **48**, 118 (1993).
[8] T. Nakamura *et al.*, Phys. Lett. B **331**, 296 (1994).
[9] T. Nakamura *et al.*, Phys. Rev. Lett. **83**, 1112 (1999).
[10] K. Alder, A. Bohr, T. Huus, B. Mottelson, and A. Winther, Rev. Mod. Phys. **28**, 432 (1956).
[11] C.A. Bertulani and G. Baur, Phys. Rep. **163**, 299 (1988).
[12] L.F. Canto, R. Donangelo, A. Romanelli, and H. Schulz, Phys. Lett. B **318**, 415 (1993).
[13] C.A. Bertulani, L.F. Canto, and M.S. Hussein, Phys. Lett. B **353**, 413 (1995).
[14] T. Kido, K. Yabana, and Y. Suzuki, Phys. Rev. C **50**, R1276 (1994).
[15] G.F. Bertsch and C.A. Bertulani, Nucl. Phys. **A556**, 136 (1993).
[16] T. Kido, K. Yabana, and Y. Suzuki, Phys. Rev. C **53**, 2296 (1996).
[17] C.A. Bertulani and G.F. Bertsch, Phys. Rev. C **49**, 2839 (1994).
[18] H. Esbensen, G.F. Bertsch, and C.A. Bertulani, Nucl. Phys. **A581**, 107 (1995).
[19] V.S. Melezhik and D. Baye, Phys. Rev. C **59**, 3232 (1999).
[20] S. Typel and R. Shyam, Phys. Rev. C **64**, 024605 (2001).
[21] S. Typel and G. Baur, Nucl. Phys. **A573**, 486 (1994).
[22] S. Typel and G. Baur, Phys. Rev. C **64**, 024601 (2001).
[23] G. Baur, F. Rösel, D. Trautmann, and R. Shyam, Phys. Rep. **111**, 333 (1984).
[24] R. Shyam, P. Banerjee, and G. Baur, Nucl. Phys. **A540**, 341 (1992).
[25] P. Banerjee, I.J. Thompson, and J.A. Tostevin, Phys. Rev. C **58**, 1042 (1998).
[26] R. Chatterjee, P. Banerjee, and R. Shyam, Nucl. Phys. **A675**, 477 (2000).
[27] R. Shyam and P. Danielewicz, Phys. Rev. C **63**, 054608 (2001).
[28] J.A. Tostevin, S. Rugmai, and R.C. Johnson, Phys. Rev. C **57**, 3225 (1998).
[29] G.G. Ohlsen, Nucl. Instrum. Methods **37**, 240 (1965).
[30] N.K. Glendenning, *Direct Nuclear Reactions* (Academic, New York, 1983).
[31] G. Baur and D. Trautmann, Nucl. Phys. **A191**, 321 (1972).
[32] G.R. Satchler, *Direct Nuclear Reactions* (Oxford University Press, New York, 1983).
[33] P. Braun-Munzinger and H.L. Harney, Nucl. Phys. **A223**, 381 (1974).
[34] R. Shyam and M.A. Nagarajan, Ann. Phys. (N.Y.) **163**, 265 (1985).
[35] D.F. Jackson, *Nuclear Reactions* (Methuen, London, 1970).
[36] A. Sommerfeld, *Atombau und Spektrallinien* (Vieweg, Braunschweig, 1939), Vol. 2.
[37] A. Nordsieck, Phys. Rev. **93**, 785 (1954).
[38] J. Lang, L. Jarczyk, and R. Müller, Nucl. Phys. **A204**, 97 (1973).
[39] E. Guth and C.J. Mullin, Phys. Rev. **83**, 667 (1951).
[40] H. van Haeringen, J. Math. Phys. **17**, 995 (1976).
[41] J. Berntsen, T.O. Espelid, and A. Genz, ACM Trans. Math. Softw. **17**, 437 (1991).